Supplementary Information:

The structural basis for MCM2-7 helicase activation by GINS and Cdc45

Alessandro Costa[1,2], Ivar Ilves[1], Nele Tamberg[1], Tatjana Petojevic[1,3], Eva Nogales[1,2,4,5], Michael R. Botchan[1,2,6] & James M. Berger[1,2,5,6]

[1] Department of Molecular and Cell Biology, University of California, Berkeley, California 94720, USA
[2] California Institute for Quantitative Biosciences, University of California, Berkeley, California, USA.
[3] Department of Biology, Chemistry, and Pharmacy, Institute of Chemistry and Biochemistry, Freie Universität Berlin, 14195 Berlin, Germany.
[4] Howard Hughes Medical Institute, University of California, Berkeley, California, USA.
[5] Life Science Division, Lawrence Berkeley National Laboratory, Berkeley, USA.
[6] Co-corresponding authors

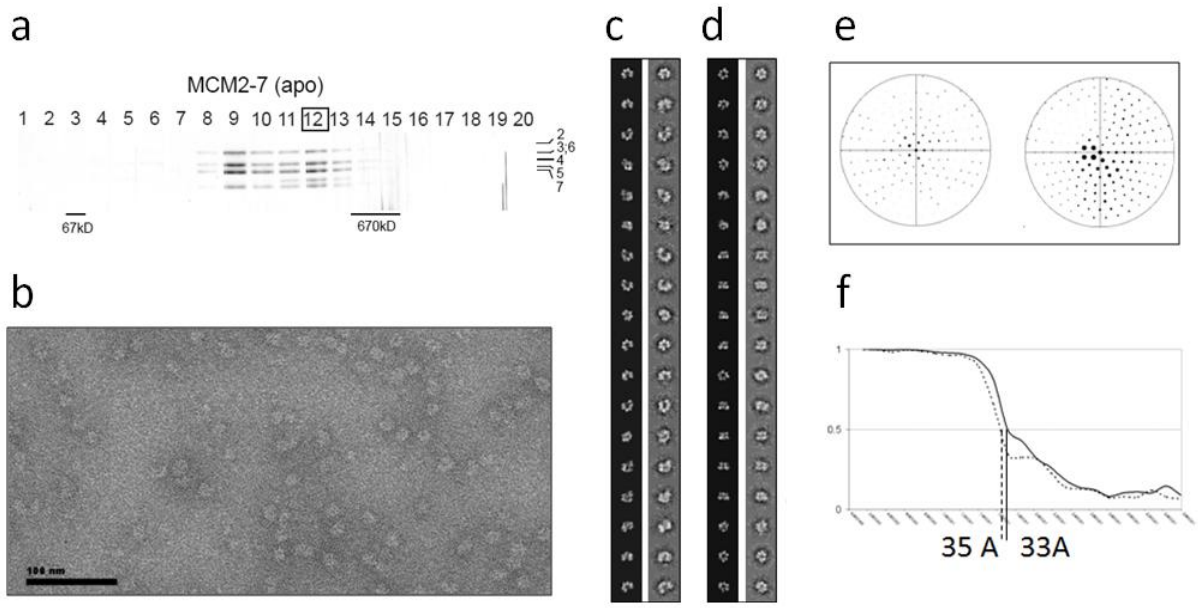

Supplementary Figure 1: Protein complex preparation and Single particle reconstruction of the *Dm*Mcm2-7 complex. All complexes were prepared as follows: proteins were expressed for two days after baculovirus co-infection of Hi5 cells (Invitrogen) in plates. Cells were treated to hypotonic shock and one round of freeze-thawing, then homogenized using Dounce homogenizer. The resulting lysate was clarified by centrifugation and flag-MCM3 containing complexes were affinity purified using anti-flag (M2) antibody-conjugated agarose beads (Sigma). To separate the stoichiometric CMG or MCM2-7 assemblies from incomplete complexes, this material was further passed through Mono S HR 5/5 and Mono Q HR 5/5 ion exchange columns on an ÄKTA Purifier FPLC system (GE Healthcare Life Sciences), and then over a Mono Q PC 1.6/5 column on a Pharmacia SMART micro-purification system. Purified samples were dialyzed into a buffer containing 25 mM HEPES (pH 7.6), 50 mM sodium acetate, 10 mM magnesium acetate, 10% glycerol and 1 mM DTT. To preserve the natural conformational states of the assembly, neither cross-linking nor intra-particle, rotational symmetry averaging was used at any point during the analysis. For our

single-particle reconstructions, we used relatively large data sets (ranging from ~7,500 to ~25,000 particles), which are necessary for multimodel refinement approaches and the projection matching of raw images[1,2]. (**a**) SDS-PAGE gel showing glycerol gradient fractions of purified *Dm*Mcm2-7. The boxed fraction was used for electron microscopy sample preparation. (**b**) Electron micrograph of apo Mcm2-7. (**c**) Forward-projections of a lockwasher structure (left) and matching reference free class averages (right). (**d**) Forward-projections of a notched-ring structure (left) and matching reference free class averages (right). (**e**) Euler angle distribution for the notched (left) and lockwasher (right) configuration. (**f**) Fourier Shell Correlation (FSC) of the notched (dashed line) or lockwasher (continuous line) structures. Resolution is indicated according to the 0.5 criterion.

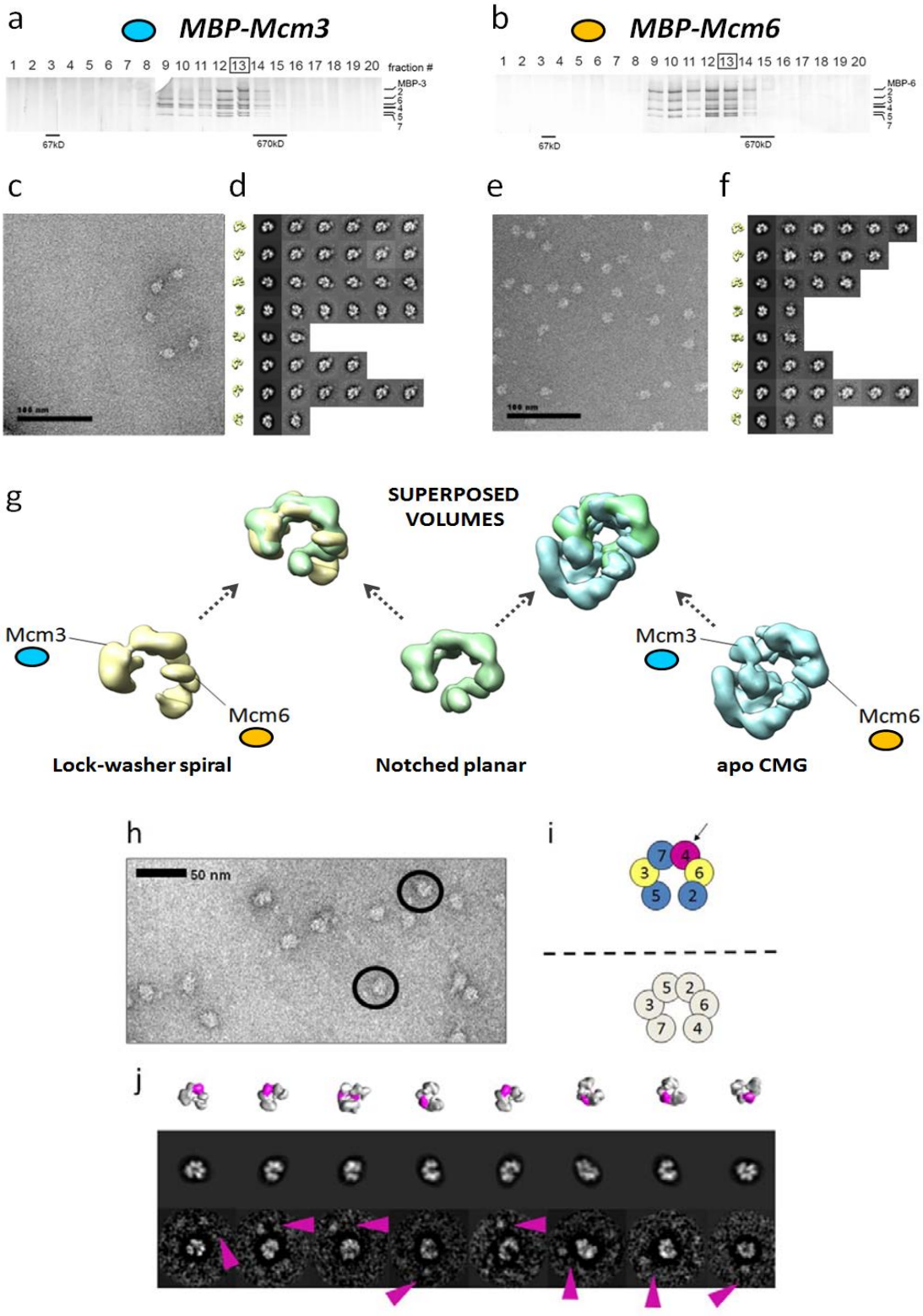
a
MBP-Mcm3
1 2 3 4 5 6 7 8 9 10 11 12 13 14 15 16 17 18 19 20 fraction #
MBP-3
67kD
670kD
b
MBP-Mcm6
1 2 3 4 5 6 7 8 9 10 11 12 13 14 15 16 17 18 19 20
MBP-6
67kD
670kD
c
d
e
f
g
SUPERPOSED VOLUMES
Mcm3
Mcm6
Lock-washer spiral
Notched planar
Mcm3
Mcm6
apo CMG
h
50 nm
i
7 4 3 6 5 2
5 2 3 6 7 4
j

Supplementary Figure 2: (a) SDS-PAGE gel showing glycerol gradient fractions of *Dm*Mcm2-7 with an N-terminal MBP tag on Mcm3, purified in the presence of ADP•BeF_3. (**b**) SDS page gel showing glycerol gradient fractions of *Dm*Mcm2-7 with an N-terminal MBP tag on Mcm6, purified in the presence of ADP•BeF_3. (**c**) Negative stain electron micrograph of ADP•BeF_3-bound *Dm*Mcm2-7 with an N-terminal MBP tag on Mcm3. (**d**) Three-dimensional structure and forward-projections of the lockwasher viewed from different directions, aligned to matching reference-free class averages of complexes bearing an N-terminal MBP tag on Mcm3. (**e**) Negative stain electron micrograph of ADP•BeF_3-bound *Dm*Mcm2-7 with an N-terminal MBP tag on Mcm6. (**f**) Three-dimensional structure and forward-projections of the lockwasher viewed from different directions, aligned to matching reference-free class averages of complexes bearing an N-terminal MBP tag on Mcm6. (**g**) Feature-based superposition of untagged Mcm2-7 and CMG volumes allows the determination of the register of the heterohexamer. In particular, one register shows the highest cross-correlation score for the Mcm2-7 lockwasher (yellow) and notched (green) configuration. A single best fitting solution was also found by superposing the apo CMG complex (cyan) and the notched Mcm2-7 configuration (green). Given these solutions, the location of the MBP tags of Mcm2-7 and CMG also match (also see **Figure 1**, **Figure 2** and **Supplementary Figure 2** and **Supplementary Figure 5**). **(h,I,j)** An N-terminal MBP tag on Mcm4 tag provides an independent assessment of the hand of Mcm2-7 subunit arrangement. Being on opposite sides of the hexameric ring structure, the N-MBP-Mcm3 and N-MBP-Mcm6 tags lie on a mirror-symmetry axis, when viewed in two dimensions. To independently determine which subunits flank the gap in the Mcm2-7 ring, we imaged the Mcm2-7 complex with an MBP tag on Mcm4, a subunit predicted to sit adjacent to Mcm6. (**h**) Negative stain electron micrograph of ADP•BeF_3-bound *Dm*Mcm2-7 complex with an N-terminal MBP tag on Mcm4. Black circles indicate rings that are clearly proximal to MBP tag densities. (**i**) Diagram showing the predicted location of Mcm4 with respect to the Mcm2-7 ring opening, considering two possible options for subunit placement, based on known pairwise interactions[3,4]; Mcm4 could be located in a position distal from the ring opening, or could be at the very opening. (**j**) Mcm2-7 lockwasher reconstructions (the orientation is the same as represented in

Supplementary Figure 2) with the predicted location of Mcm4 highlighted in magenta are shown at top. Forward-projections of the structure, along the same views are shown in the middle panel, with reference free class averages aligned to the forward projections shown at the bottom. The arrowhead in magenta highlights the location of the MBP density. The Mcm4 MBP-tag appears distal from the center of the protein-complex density and opposite the ring opening. This configuration indicates that the N-terminal domain of Mcm4 is elongated and likely partly unstructured, in agreement with indications derived from secondary structure prediction.

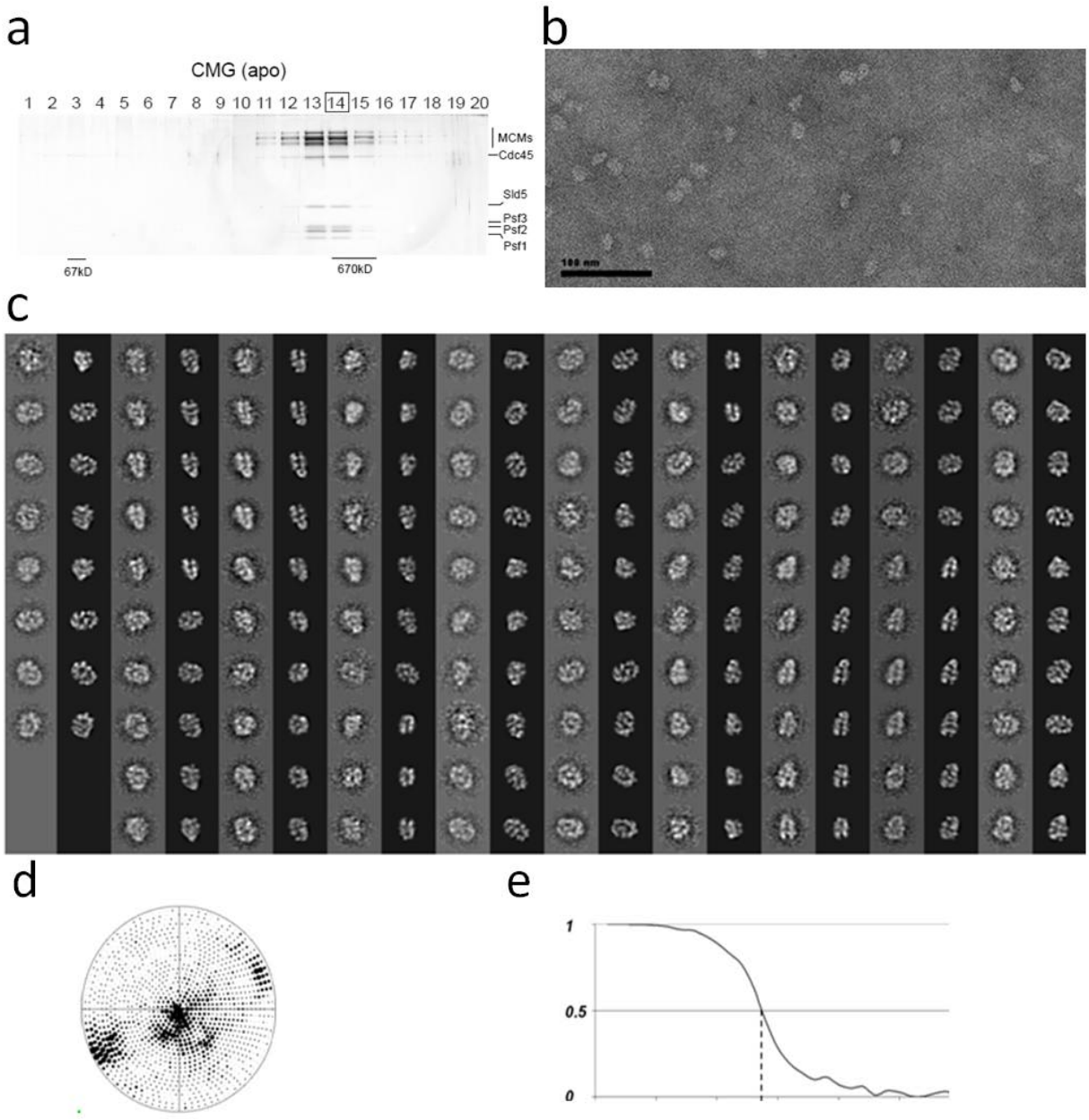

Supplementary Figure 3: Single particle reconstruction of apo *Dm*CMG. (**a**) SDS-PAGE gel showing glycerol gradient fractions of purified apo *Dm*CMG. (**b**) Electron micrograph of the apo CMG complex. (**c**) Reference-free class averages (grey background) and matching forward-projections of the three-dimensional structure (black

background). (**d**) Euler angle distribution. (**e**) FSC indicating a resolution of 27.6 Å, according to the 0.5 criterion.

a

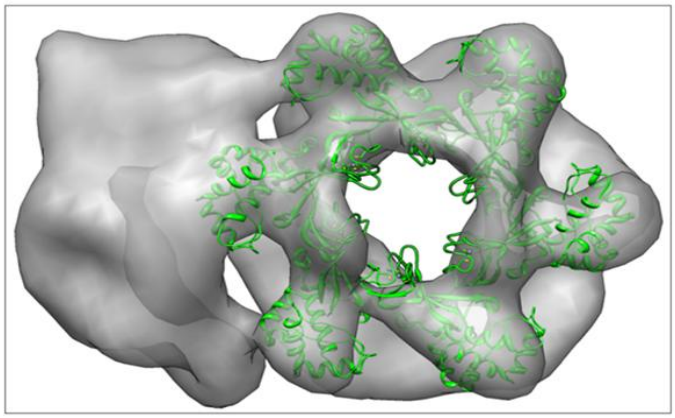

b

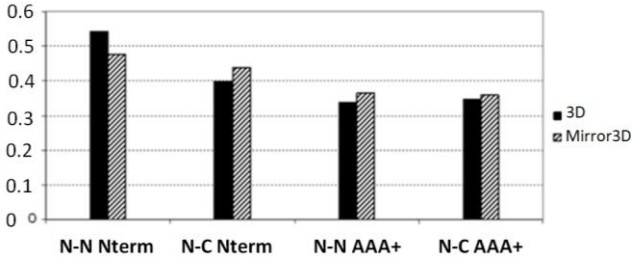
0.6
0.5
0.4
0.3
0.2
0.1
0
N-N Nterm
N-C Nterm
N-N AAA+
N-C AAA+
3D
Mirror3D

c

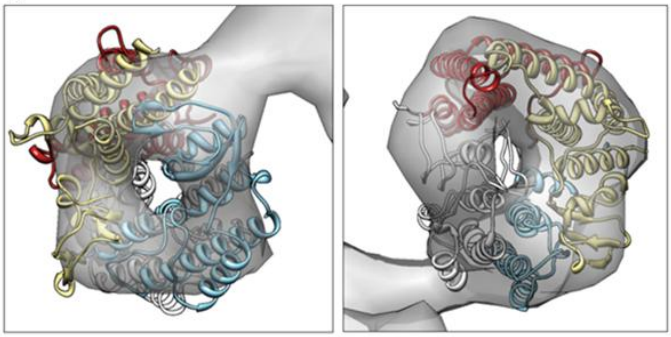

d

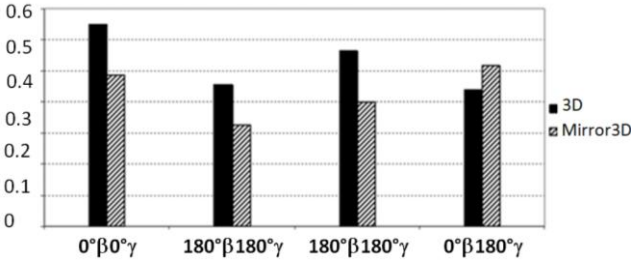
0.6
0.5
0.4
0.3
0.2
0.1
0
0°β0°γ
180°β180°γ
180°β180°γ
0°β180°γ
3D
Mirror3D

Supplementary Figure 4: Determination of the handedness of the ADP•BeF_3-bound CMG by fitting of the atomic structures into the two subcomplexes. (**a**) The hexameric *Mth*MCM N-terminal domain, fit automatically using Chimera[5] into the ADP•BeF_3-bound CMG reconstruction. (**b**) Plot indicating the score for the fitting of an *Mth*MCM N-terminal domain hexamer (PDB entry:1LTL[6]) in eight possible configurations within the CMG complex. A cross-correlation coefficient (CCC) was calculated for both hands of the map ("3D" or "mirror 3D"), both faces of the *Mth*MCM ring ("N-" or "C-") and both tiers of the eukaryotic Mcm2-7 ring ("-N" or "-C"). The best solution locates the N-terminal domains of the Mcm2-7 in a position that is in agreement with the location of the N-terminally fused MBP tags seen in our single particle reconstructions (Figure 2). (**c**) Two details of the fitting of the atomic structure of human GINS (PDB: 2Q9Q[7]) into the lateral electron density appendix of the *Dm*CMG structure. (**d**) A plot indicating the score for the fitting of the atomic coordinates in eight possible configurations of GINS within the CMG complex, considering two different hands ("3D" or "mirror 3D"), two possible orientations given by the rotation about the long axis of the GINS electron density ("0°β" or "180°β") and two possible orientations given by the rotation about the short axis of the GINS electron density ("0°γ" or "180°γ").

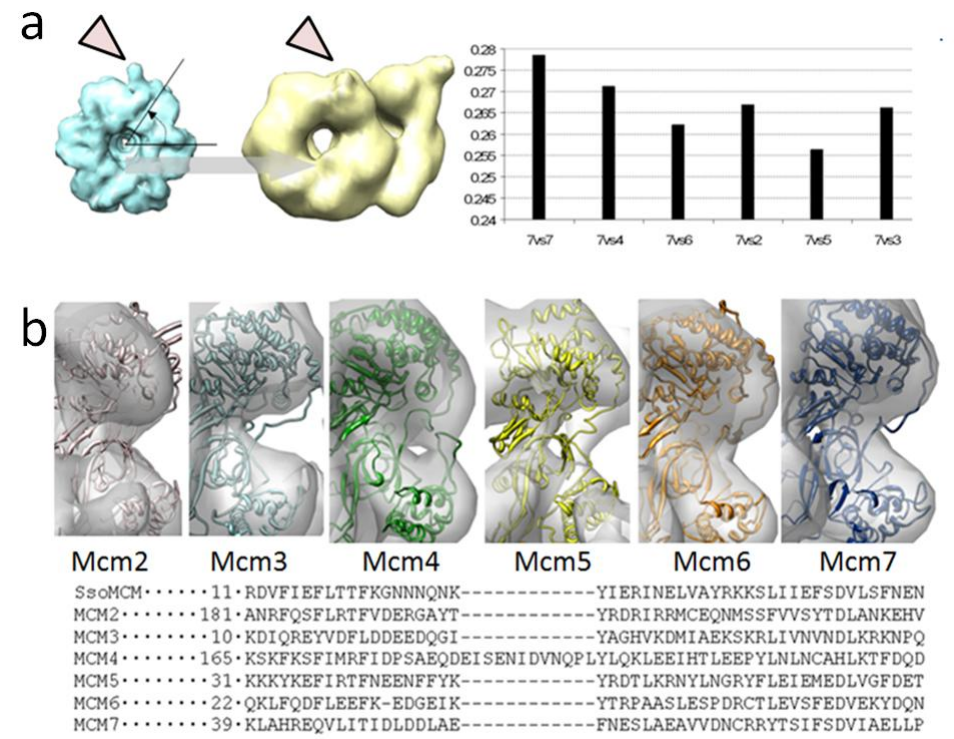
a
0.28
0.275
0.27
0.265
0.26
0.255
0.25
0.245
0.24
7vs7
7vs4
7vs6
7vs2
7vs5
7vs3
b
Mcm2
Mcm3
Mcm4
Mcm5
Mcm6
Mcm7
SsoMCM·····11·RDVFIEFLTTFKGNNNQNK----------YIERINELVAYRKKSLIIEFSDVLSFNEN
MCM2·····181·ANRFQSFLRTFVDERGAYT----------YRDRIRRMCEQNMSSFVVSYTDLANKEHV
MCM3·····10·KDIQREYVDFLDDEEDQGI----------YAGHVKDMIAEKSKRLIVNVNDLKRKNPQ
MCM4·····165·KSKFKSFIMRFIDPSAEQDEISENIDVNQPLYLQKLEEIHTLEEPYLNLNCAHLKTFDQD
MCM5·····31·KKKYKEFIRTFNEENFFYK----------YRDTLKRNYLNGRYFLEIEMEDLVGFDET
MCM6·····22·QKLFQDFLEEFK-EDGEIK----------YTRPAASLESPDRCTLEVSFEDVEKYDQN
MCM7·····39·KLAHREQVLITIDLDDLAE----------FNESLAEAVVDNCRRYTSIFSDVIAELLP
c
50 nm
d
7
4
3
6
5
2
5
2
3
6
7
4
e

Supplementary Figure 5: Determination of the register of Mcm subunits within the CMG complex.

(**a**) Electron density map of a modeled Mcm2-7 hetero-hexamer (left, based on homology models to the archaeal Mcm crystal structure[8]), the ADP•BeF_3-bound CMG structure (center) and a plot of rotational correlation score (right). (**b**) Homology models for each of the six Mcm subunits fitted into the ADP•BeF_3-bound CMG map (top), along with a sequence alignment of the six N-terminal A-domains.

After the handedness of the ADP•BeF_3 CMG map was determined as detailed in **Supplementary Figure 4,** rotational correlation function was used to determine the register of Mcm2-7 subcomplex within the CMG. In this approach, homology models for the six individual Mcm2-7 subunits were built as detailed in the Methods section, based on the full-length archaeal MCM monomer (PDB entry: 3F8T[8]) and then superposed, using known pairwise subunit interactions[3,4], onto the structure of the hexameric N-terminal domain tier of the *Mth*MCM (PDB entry: 1LTL[6] to generate a model for the *Dm*Mcm2-7 heterohexamer. Next, an electron density map was calculated from this atomic structure, using the same sampling frequency used for EM data collection (5.72 Å/pixel). A cross-correlation function (as implemented in Chimera[5] was used to assay the six possible superposition registers of the CMG structure with the modeled hetero-hexamer. One register gave the highest cross-correlation score (a), which was in agreement with our reconstructions of MBP-tagged Mcm6 and Mcm3 variants of ADP•BeF_3-bound CMG. Two features can be recognized in the single-particle generated and atomic-model derived electron density maps, which suggest one preferred register. One is a predicted beta hairpin that departs radially from the AAA+ domain of Mcm2, resulting in a bump at the periphery of the Mcm2-7 upper tier (indicated by a pink arrowhead in panel a). The other is a loop insertion departing from the N-terminal subdomain A, which is unique to Mcm4 (panel b). This inserted loop fits some additional side density, thickening the "waist" between the N- and C-terminal tiers, and connecting the outer perimeter of the AAA+ and N-terminal tiers of Mcm4 (see panel B and **Supplementary Movie 2**).

To further confirm our Mcm subunit assignment we examined a N-terminal, MBP-tagged ADP•BeF_3-boundCMG complex. Panel (**c**) shows a micrograph where a characteristic side and top views are highlighted by a black circle. Inspection of raw images indicates a position for Mcm4 based on location of MBP that departs from a central location in the CMG complex, distal to the electron density occupied by GINS and Cdc45. (**d**) A diagram summarizing the conclusive determination of the subunit register and hand of the CMG map, based solely on MBP tag mapping.

(**e**) Different views of the ADP•BeF_3 CMG reconstruction with the location of Mcm4 highlighted in magenta, as predicted from the localization of subunits Mcm6 and Mcm3 (**Figure 2**) and rotational correlation function approaches (panel A of this Figure). Forward projections of the three-dimensional structure along the same directional cosine vectors are shown (black background), as are matching reference-free class averages showing density for the N-terminal MBP in a position compatible with the predicted location of Mcm4 (stippled background).

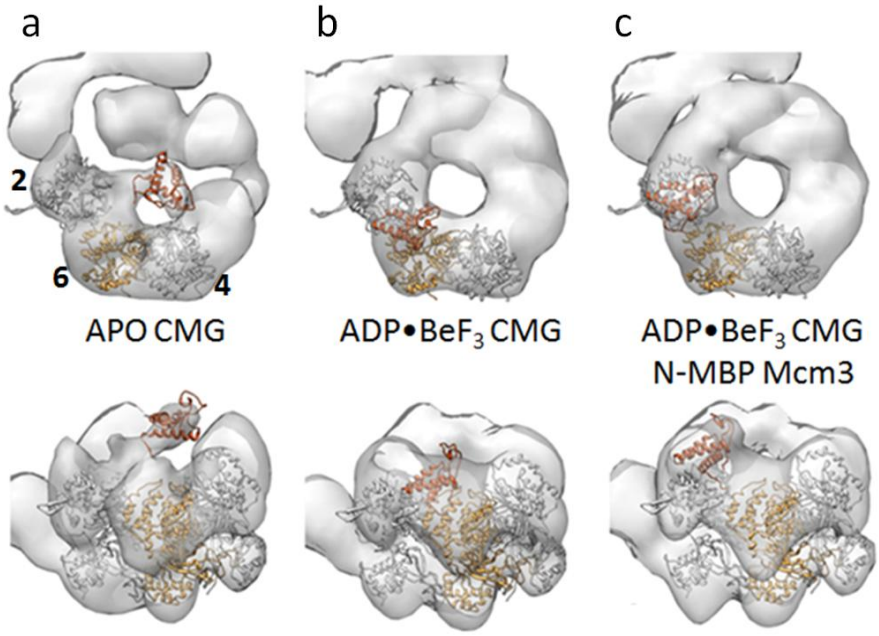

Supplementary Figure 6: Proposed location of the C-terminal Winged Helix Domain of Mcm6. (**a**) Top and side views of the apo CMG structure displayed at lower contour levels with fitted Mcm2 (grey), Mcm6 (gold) and Mcm4 (grey) models. The Mcm6 WHD structure (PDB entry: 2KLQ)[9] is shown in dark gold. (**b**) Top and side views of the ADP•BeF_3-bound CMG with fitted atomic coordinates following the same color scheme. (**c**) Top and side views of the ADP•BeF_3-bound CMG, with an N–terminal MBP tag on Mcm3.

When apo CMG is displayed at lower contour level, additional electron density appears to depart from the AAA+ face of the Mcm6 subunit and project to the top of the Mcm2-7 central channel, effectively capping the ring and potentially providing a steric impediment to DNA binding in the centre of the channel. Mcm6 is known to contain a C-terminal Winged helix domain (WHD), whose atomic coordinates can be placed into this additional electron density, using the "Fit-in-volume" function in Chimera[5]. Archaeal MCMs are also believed to contain a C-terminal WHD[10], and a similar position for the C-terminal WHD of the *Mth*MCM has previously been proposed based on single particle

reconstruction studies [11]. Noticeably, a deletion of this domain in *Mth*MCM showed increased DNA binding properties *in vitro*[12], in agreement with the notion that WHD might control nucleic acid accessibility to the central channel. Upon binding to ADP•BeF_3, the Mcm6 WHD cap becomes recessed and/or partially unstructured, adopting an alternate configuration similar to that observed in a cryo-EM study of the *Mth*MCM protein complex[13]. A somewhat intermediate configuration for the same element can be observed in ADP•BeF_3 CMG complex with the N-terminal MBP tagged Mcm3. In this reconstruction, additional density likely corresponding to a structured and recessed WHD can be observed, extruding from the interface between Mcm2 and Mcm6 AAA+ domains in a region otherwise corresponding to a depression in the apo CMG electron density map. Note that the placement of this domain is meant only to serve as a rough guide to its likely relative positions; the present reconstructions lack the resolution to determine an absolute orientation for the WHD in the observable density.

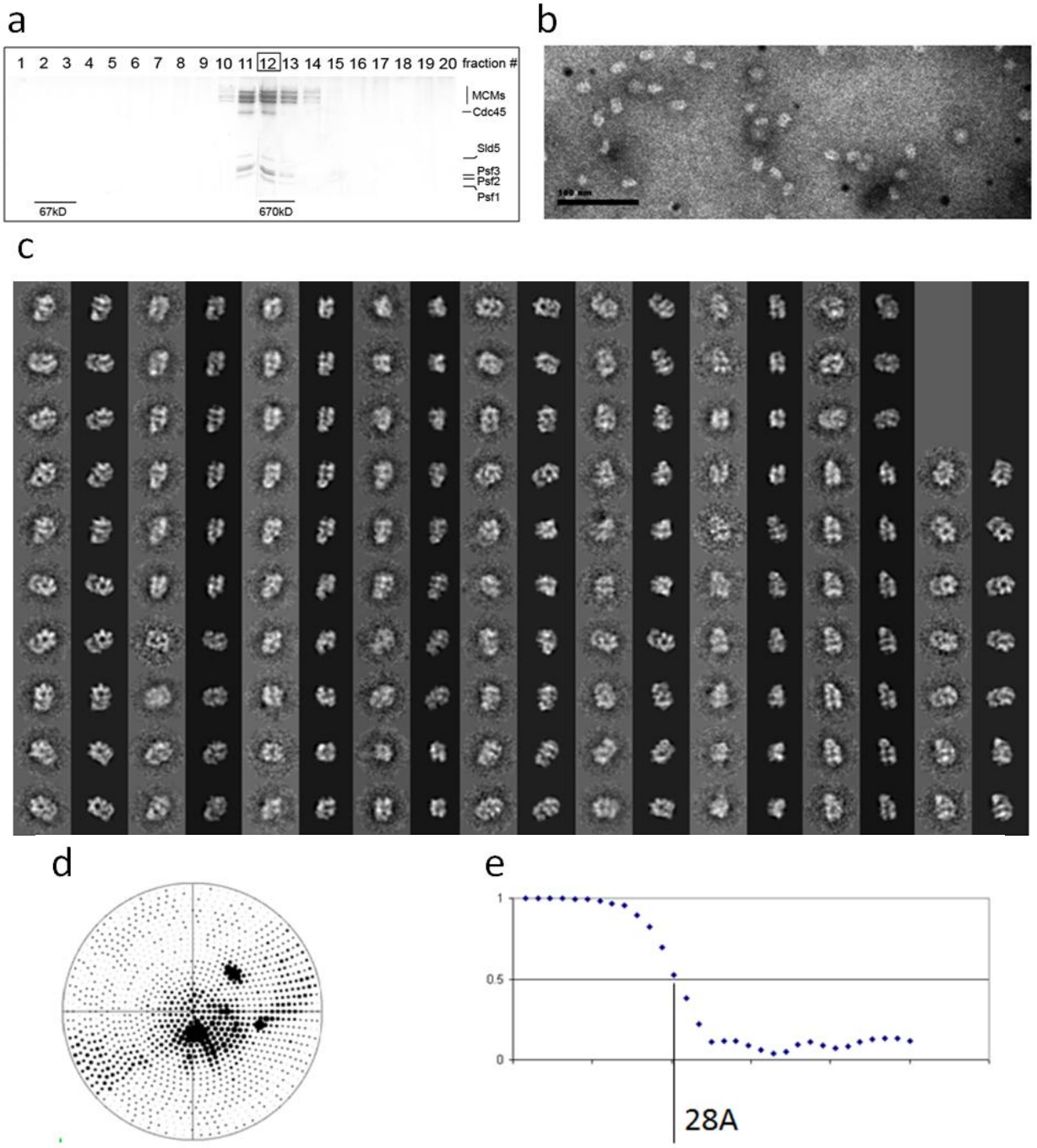

Supplementary Figure 7: Single particle reconstruction of the ADP•BeF_3-bound *Dm*CMG. (**a**) SDS-PAGE gel showing glycerol gradient fractions of purified ADP•BeF_3-bound *Dm*CMG. (**b**) Electron micrograph of the complex. (**c**) Forward-projections of the three-dimensional structure (black background) and matching reference-free class

averages (grey background). (**d**) Euler angle distribution. (**e**) FSC indicating a resolution of 28 Å, according to the 0.5 criterion.

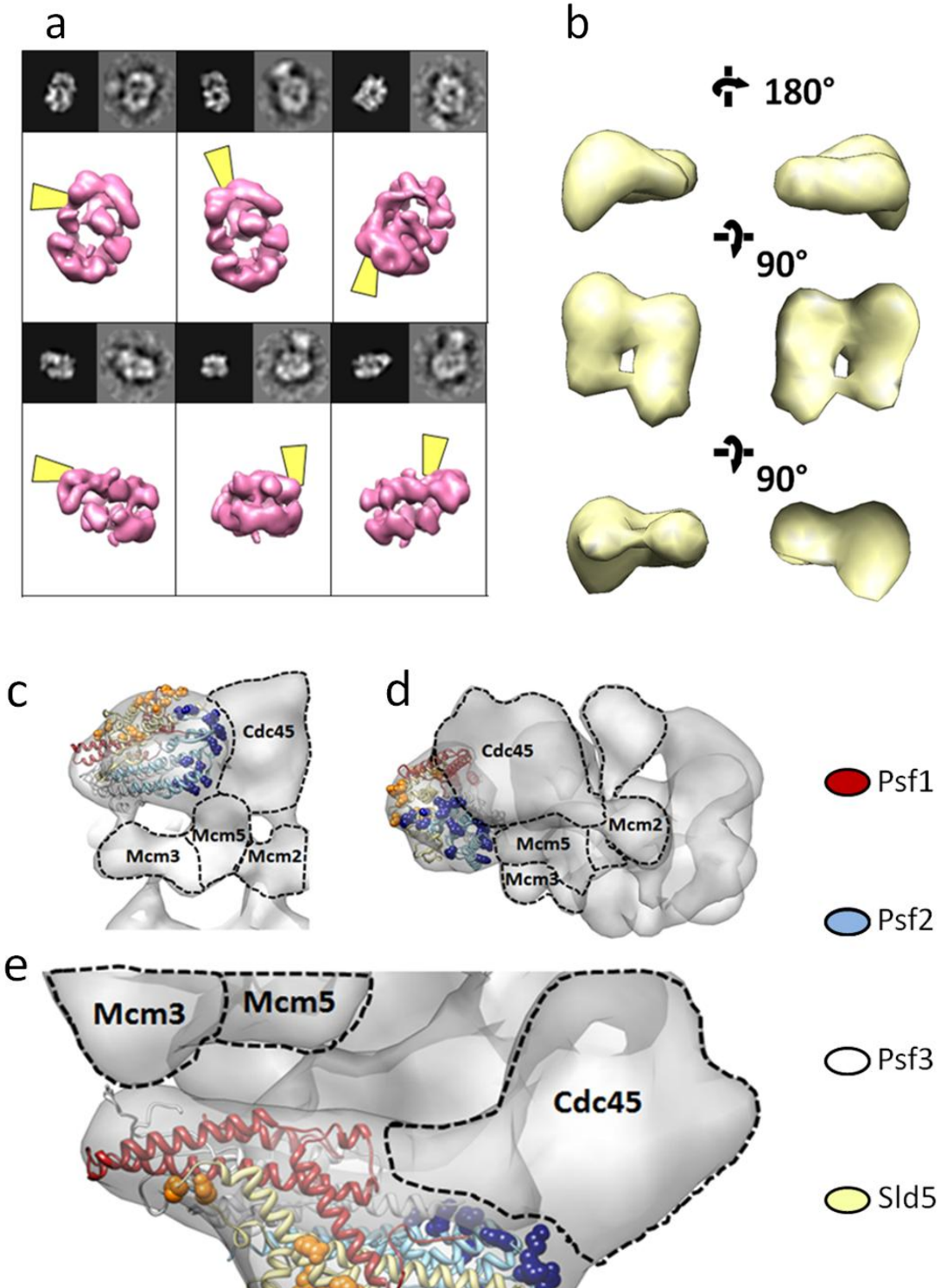
a
b
180°
90°
90°
c
Cdc45
Mcm5
Mcm3
Mcm2
d
Cdc45
Mcm2
Mcm5
Mcm3
Psf1
Psf2
e
Mcm3
Mcm5
Cdc45
Psf3
Sld5

Supplementary Figure 8: (**a-b**)Global shape and architectural role of *Dm*Cdc45**.** (**a**) Forward projections of the apo CMG reconstruction (black background) followed by matching reference-free class averages of anti-Cdc45-antibody bound CMG. The electron density map of CMG is shown in pink with a flag indicating the position of the extra-electron density that likely corresponds to a Fab domain bound to the Cdc45 subunit. This additional density consistently maps proximally to the side-handle electron density feature of the CMG, which model fitting suggests is partially occupied by GINS. (**b**) The low resolution structure of Cdc45, obtained after subtracting the density corresponding to Mcm2-7 and GINS from the apo CMG structure. Cdc45 appears to be composed of two distinct globular domains separated by a narrow groove. (**c, d, e**) Conserved surface residues on GINS essential for viability, mapped onto the CMG. (**c**) Bottom (Mcm2-7 N-terminal) (**d**) side and (**e**) top (Mcm2-7 C-terminal) view of ADP•BeF_3-bound CMG fitted with atomic coordinates of human GINS [7]. Predicted locations for Cdc45, Mcm3 and Mcm5 are indicated with a dashed line. Psf1 is shown in dark red, Psf2 in light blue, Psf3 in white, Sld5 in yellow. Corresponding residues identified as essential for yeast cells viability[14] are shown as dark blue (in Psf2) or orange (Sld5). An extensive surface in Psf2 essential for viability corresponds to the point of contact with Cdc45 and Subdomain A of the N-terminal Mcm5. The N-terminal region of Sld5 also was characterized as essential for viability, but does not appear to be involved in any inter-subunit interaction contact in the CMG; this region may be involved in the binding of other interaction partners in the RPC.

Supplentary bibliography

1. Shaikh, T.R. et al. SPIDER image processing for single-particle reconstruction of biological macromolecules from electron micrographs. *Nat Protoc* **3**, 1941-74 (2008).
2. Grob, P. et al. Cryo-electron microscopy studies of human TFIID: conformational breathing in the integration of gene regulatory cues. *Structure* **14**, 511-20 (2006).
3. Davey, M.J., Indiani, C. & O'Donnell, M. Reconstitution of the Mcm2-7p heterohexamer, subunit arrangement, and ATP site architecture. *J Biol Chem* **278**, 4491-9 (2003).
4. Crevel, G., Ivetic, A., Ohno, K., Yamaguchi, M. & Cotterill, S. Nearest neighbour analysis of MCM protein complexes in Drosophila melanogaster. *Nucleic Acids Res* **29**, 4834-42 (2001).
5. Pettersen, E.F. et al. UCSF Chimera--a visualization system for exploratory research and analysis. *J Comput Chem* **25**, 1605-12 (2004).
6. Fletcher, R.J. et al. The structure and function of MCM from archaeal *M. thermoautotrophicum*. *Nat Struct Biol* **10**, 160-7 (2003).
7. Chang, Y.P., Wang, G., Bermudez, V., Hurwitz, J. & Chen, X.S. Crystal structure of the GINS complex and functional insights into its role in DNA replication. *Proc Natl Acad Sci U S A* **104**, 12685-90 (2007).
8. Brewster, A.S. et al. Crystal structure of a near-full-length archaeal MCM: functional insights for an AAA+ hexameric helicase. *Proc Natl Acad Sci U S A* **105**, 20191-6 (2008).
9. Wei, Z. et al. Characterization and structure determination of the Cdt1 binding domain of human minichromosome maintenance (Mcm) 6. *J Biol Chem* **285**, 12469-73.
10. Aravind, L. & Koonin, E.V. DNA-binding proteins and evolution of transcription regulation in the archaea. *Nucleic Acids Res* **27**, 4658-70 (1999).
11. Costa, A. et al. Structural basis of the *Methanothermobacter thermautotrophicus* MCM helicase activity. *Nucleic Acids Res* **34**, 5829-38 (2006).
12. Jenkinson, E.R. & Chong, J.P. Minichromosome maintenance helicase activity is controlled by N- and C-terminal motifs and requires the ATPase domain helix-2 insert. *Proc Natl Acad Sci U S A* **103**, 7613-8 (2006).
13. Costa, A. et al. Cryo-electron microscopy reveals a novel DNA-binding site on the MCM helicase. *Embo J* **27**, 2250-8 (2008).
14. Choi, J.M., Lim, H.S., Kim, J.J., Song, O.K. & Cho, Y. Crystal structure of the human GINS complex. *Genes Dev* **21**, 1316-21 (2007).